

Design and Synthesis of a Fluorescent Probe for Zn^{2+} , 5,7-Bis(*N,N*-dimethylaminosulfonyl)-8-hydroxyquinoline-Pendant 1,4,7,10-Tetraazacyclododecane and Zn^{2+} -Dependent Hydrolytic and Zn^{2+} -Independent Photochemical Reactivation of Its Benzenesulfonyl-Caged Derivative

Ryosuke Ohshima,[†] Masanori Kitamura,^{†,‡} Akinori Morita,[§] Motoo Shiro,^{||} Yasuyuki Yamada,[†] Masahiko Ikekita,[§] Eiichi Kimura,[⊥] and Shin Aoki^{*,†,‡}

[†]*Faculty of Pharmaceutical Sciences, Tokyo University of Science, 2641 Yamazaki, Noda 278-8510, Japan,*

[‡]*Center for Technologies against Cancer, Tokyo University of Science, 2641 Yamazaki, Noda 278-8510, Japan,*

[§]*Faculty of Science and Technology, Tokyo University of Science, 2641 Yamazaki, Noda 278-8510, Japan,*

^{||}*Rigaku Corporation X-ray Research Laboratory, 3-9-12 Matsubaracho, Akishima, Tokyo 196-8666, Japan,*

and [⊥]*Faculty of Science, Shizuoka University, 836 Ohya, Suruga-ku, Shizuoka 422-8529, Japan*

Received July 15, 2009

We previously reported on a 8-quinolinol-pendant cyclen (L^5) as a Zn^{2+} fluorophore (cyclen = 1,4,7,10-tetraazacyclododecane) and its caged derivative, 8-(benzenesulfonyloxy)-5-(*N,N*-dimethylaminosulfonyl)quinolin-2-ylmethyl-pendant cyclen (BS-caged- L^5), which can be reactivated by hydrolysis of benzenesulfonyl group upon complexation with Zn^{2+} at neutral pH to give a 1:1 Zn^{2+} – L^5 complex ($\text{Zn}(\text{H}_{-1}\text{L}^5)$). We report herein on the synthesis of 5,7-bis(*N,N*-dimethylaminosulfonyl)-8-hydroxyquinolin-2-ylmethyl-pendant cyclen (L^6) and its caged derivative (BS-caged- L^6) for more sensitive and more efficient cell-membrane permeability than those of L^5 and BS-caged- L^5 . By potentiometric pH, ^1H NMR, and UV–vis spectroscopic titrations, the deprotonation constants $\text{p}K_{\text{a}1}$ – $\text{p}K_{\text{a}6}$ of H_5L^6 were determined to be <2, <2, <2, 2.5 ± 0.1 (for the 8-OH group of the quinoline moiety), 9.7 ± 0.1 , and 10.8 ± 0.1 at 25 °C with $I = 0.1$ (NaNO_3). The results of ^1H NMR, potentiometric pH, UV–vis, and fluorescent titrations showed that L^6 rapidly forms a 1:1 complex with Zn^{2+} ($\text{Zn}(\text{H}_{-1}\text{L}^6)$), the dissociation constant of which is 50 fM at pH 7.4. The fluorescent emission of $\text{Zn}(\text{H}_{-1}\text{L}^6)$ at 478 nm is 32 times as large as that of L^6 (excitation at 370 nm), and the fluorescent quantum yield of $\text{Zn}(\text{H}_{-1}\text{L}^6)$ ($\Phi_{\text{F}} = 0.41$) is much greater than that of $\text{Zn}(\text{H}_{-1}\text{L}^5)$ ($\Phi_{\text{F}} = 0.044$). The BS-caged- L^6 was reactivated by hydrolysis of the benzenesulfonyl moiety more rapidly (completes in 30 min at pH 7.4 at 37 °C) than BS-caged- L^5 , presumably enabling the practical detection of Zn^{2+} in sample solutions and living cells. The photochemical deprotection of BS-caged- L^6 and the cell membrane permeability of L^6 and BS-caged- L^6 are also described.

Introduction

Zn^{2+} is one of the indispensable metal ions in living systems, and its biological roles in Zn^{2+} enzymes, DNA and RNA synthesis, gene expression, and so on have been

extensively studied.¹ In recent years, a variety of additional functions of free Zn^{2+} as a neural signal transmitter² and a key intracellular regulator of apoptosis³ have been revealed. Therefore, the development of sensitive Zn^{2+} sensors based

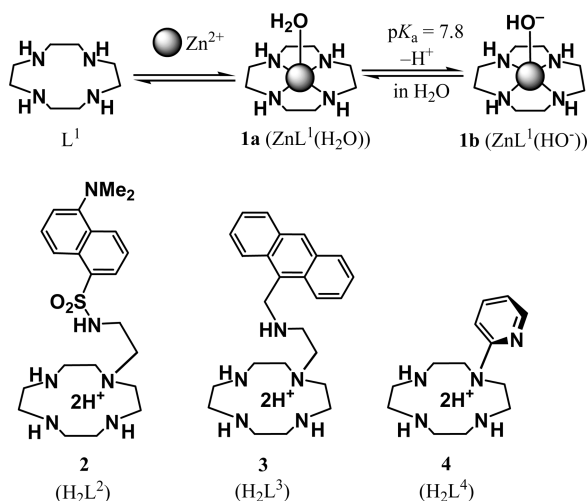
*To whom correspondence should be addressed. E-mail: shinaoki@rs.noda.tus.ac.jp.

(1) (a) Auld, D. A. In *Handbook of Metalloprotein*; Bertini, I., Sigel, A., Sigel, H., Eds.; Marcel Dekker: New York, 2001; pp 881–959. (b) Auld, D. S. *BioMetals* **2001**, *14*, 271–313. (c) Pabo, C. O.; Peisach, E.; Grant, R. A. *Annu. Rev. Biochem.* **2001**, *70*, 313–340. (d) Aoki, S.; Kimura, E. In *Comprehensive Coordination Chemistry II*; Que, L., Jr., Tolman, W. B., Eds.; Elsevier: Amsterdam, 2004; Vol. 8, pp 601–640. (e) Maret, W. *J. Trace Elem. Med. Biol.* **2005**, *19*, 7–12. (f) Papworth, M.; Kolasinska, P.; Minczuk, M. *Gene* **2005**, *366*, 27–38. (g) Ye, B.; Maret, W.; Vallee, B. L. *Proc. Natl. Acad. Sci. U.S.A.* **2005**, *98*, 2317–2322.

(2) (a) Cuajungco, M. P.; Lees, G. J. *Neurobiol. Dis.* **1997**, *4*, 137–169. (b) Choi, D. W.; Koh, J. Y. *Annu. Rev. Neurosci.* **1998**, *21*, 347–375. (c) Frederickson, C. J.; Bush, A. I. *BioMetals* **2001**, *14*, 353–366. (d) Takeda, A. *BioMetals* **2001**, *14*, 343–351. (e) Burdette, S. C.; Lippard, S. J. *Coord. Chem. Rev.* **2001**, *216–217*, 333–361. (f) Burdette, S. C.; Lippard, S. J. *Proc. Natl. Acad. Sci. U.S.A.* **2003**, *100*, 3605–3610.

(3) (a) Treves, S.; Trentini, P. L.; Ascannelli, M.; Bucci, G.; Di Virgilio, F. *Exp. Cell Res.* **1994**, *211*, 339–343. (b) Perry, D. K.; Smyth, M. J.; Stennicke, H. R.; Salvesen, G. S.; Duriez, P.; Poirier, G. G.; Hannun, Y. A. *J. Biol. Chem.* **1997**, *272*, 18530–18533. (c) Chai, F.; Truong-Tran, A. Q.; Ho, L. H.; Zalewski, P. D. *Immuno. Cell. Biol.* **1999**, *77*, 272–278. (d) Truong-Tran, A. Q.; Carter, J.; Ruffin, R. E.; Zalewski, P. D. *BioMetals* **2001**, *14*, 315–330.

Scheme 1

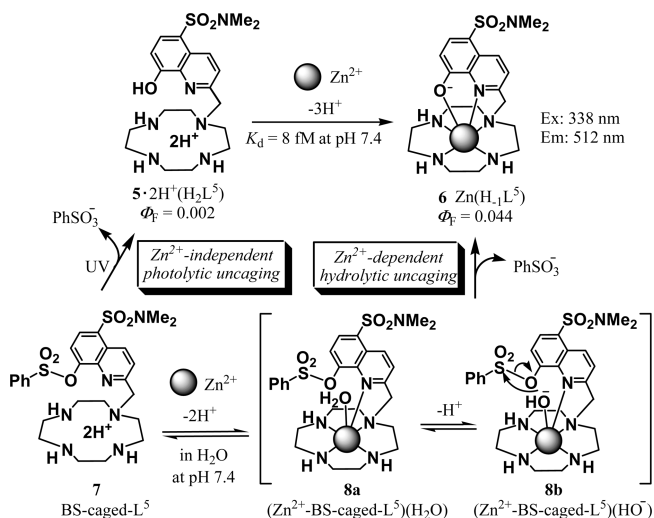


on chelation-enhanced fluorescent mechanisms is currently of great interest.^{4,5}

It has been established that 1,4,7,10-tetraazacyclododecane (cyclen, L¹) forms a very stable Zn²⁺ complex **1** (ZnL¹)⁶ in aqueous solution at neutral pH (Scheme 1) and is a potential platform for Zn²⁺-selective fluorophores^{4a,c} such as **2** (L²),⁷ **3** (L³),⁸ **4** (L⁴).⁹

We recently reported on a Zn²⁺ fluorophore **5** (L⁵)¹⁰ bearing 5-*N,N*-dimethylamino-8-hydroxyquinoline and cyclen moieties (Scheme 2). The fluorescent emission of **5** increased by a factor of 22 upon complexation with Zn²⁺ (quantum yields (Φ_F) for the emission of **5** and **6** are 2.0 × 10⁻³ and 4.4 × 10⁻²). In addition, it was found that **5** forms a very stable Zn²⁺ complex **6** (Zn(H₁L⁵)) in aqueous solution

Scheme 2



(K_d = 8 fM at pH 7.4) and that its Zn²⁺ complexation is complete in the order of milliseconds. A “caged (chemically protected)” derivative of **5**, **7** (BS-caged-L⁵), was recently synthesized, in attempts to improve Zn²⁺/Cd²⁺ selectivity and cell-membrane permeability (Scheme 2).¹¹ It was found that **7** forms a Zn²⁺ complex **8** Zn²⁺-BS-caged-L⁵ and that the Zn²⁺-bound H₂O in **8a** was deprotonated to afford Zn²⁺-HO⁻ species in **8b**, which promoted the hydrolysis of the benzenesulfonyl group, resulting in the formation of **6** (Zn(H₁L⁵)) (Zn²⁺-dependent hydrolytic uncaging). While Zn²⁺/Cd²⁺ selectivity was not improved, considerable enhancement in cellular uptake was achieved. In addition, we happened to find that the photoirradiation of **7** promotes the photochemical hydrolysis of its sulfonate moiety to yield **5** and benzenesulfonate (PhSO₃⁻) in the absence and presence of Zn²⁺ (Zn²⁺-independent photolytic uncaging).

In this work, we wish to report on the synthesis of 5,7-bis(*N,N*-dimethylaminosulfonyl)-8-hydroxyquinolin-2-ylmethyl-pendant cyclen **10** (L⁶) (Scheme 3). It had previously been reported that 5,7-bis(*N,N*-dimethylaminosulfonyl)-2-methyl-8-quinolinol **9b** has a much greater quantum yield for emission (Φ_F = 0.70) than that (Φ_F = 0.24) of **9a**.¹² Therefore, it was expected that **10** (L⁶) would be a more sensitive Zn²⁺ probe than **5** (L⁵). In this manuscript, we describe the chemical and photochemical behaviors of **10** and the Zn²⁺-dependent hydrolytic and Zn²⁺-independent photochemical reactions of the caged derivative **12** (BS-caged-L⁶). Data on the intracellular concentrations of **10** and **12** and the staining of Zn²⁺-loaded living cells with these probes are also presented.

Experimental Section

General Information. Reagents and solvents were purchased at the highest commercial quality and were used without further purification. *N*-bromosuccinimide (NBS) was recrystallized from water before use. ZnSO₄·7H₂O, Zn(NO₃)₂·6H₂O, 3CdSO₄·8H₂O, CuSO₄·5H₂O, CoSO₄·7H₂O, FeSO₄·7H₂O, AgNO₃, FeCl₃·6H₂O, KCl, MgSO₄, and CaSO₄·2H₂O were

(4) Reviews: (a) Kimura, E.; Koike, T. *Chem. Soc. Rev.* **1998**, 27, 179–184. (b) Prodi, L.; Bolletta, F.; Montalti, M.; Zaccaroni, N. *Coord. Chem. Rev.* **2000**, 205, 59–83. (c) Kimura, E.; Aoki, S. *BioMetals* **2001**, 14, 191–204. (d) Kikuchi, K.; Komatsu, K.; Nagano, T. *Curr. Opin. Chem. Biol.* **2004**, 8, 182–191. (e) Jiang, P.; Guo, Z. *Coord. Chem. Rev.* **2004**, 248, 205–229. (f) Dai, Z.; Canary, J. W. *New J. Chem.* **2007**, 31, 1708–1718. (g) Nolan, E. M.; Lippard, S. J. *Acc. Chem. Res.* **2009**, 42, 193–203.

(5) For recent examples, see: (a) Burdette, S. C.; Lippard, S. J. *Proc. Natl. Acad. Sci. U.S.A.* **2003**, 100, 3605–3610. (b) Woodrooffe, C. C.; Masalha, R.; Barnes, K. R.; Frederickson, C. J.; Lippard, S. J. *Chem. Biol.* **2004**, 11, 1659–1666. (c) Kiyose, K.; Kojima, H.; Urano, Y.; Nagano, T. *J. Am. Chem. Soc.* **2006**, 128, 6548–6549. (d) Harriman, A.; Mallon, L. J.; Stewart, B.; Ulrich, G.; Ziessel, R. *Eur. J. Org. Chem.* **2007**, 3191–3198. (e) Parkesh, R.; Lee, T. C.; Gunnlaugsson, T. *Org. Biomol. Chem.* **2007**, 5, 310–317. (f) Atilgan, S.; Ozdemir, T.; Akkaya, E. U. *Org. Lett.* **2008**, 10, 4065–4067. (g) Zhang, Y.; Guo, X.; Si, W.; Jia, L.; Qian, X. *Org. Lett.* **2008**, 10, 473–476. (h) Alarcón, J.; Albelda, M. T.; Belda, R.; Clares, M. P.; Delgado-Pinar, E.; Frías, J. C.; García-España, E.; González, J.; Soriano, C. *Dalton Trans.* **2008**, 6530–6538. (i) Qian, F.; Zhang, C.; Zhang, Y.; He, W.; Gao, X.; Hu, P.; Guo, Z. *J. Am. Chem. Soc.* **2009**, 131, 1460–1468. (j) Tamanini, E.; Katewa, A.; Sedger, L. M.; Todd, M. H.; Watkinson, M. *Inorg. Chem.* **2009**, 48, 319–324.

(6) (a) Kimura, E.; Shiota, T.; Koike, T.; Shiro, M.; Kodama, M. *J. Am. Chem. Soc.* **1990**, 112, 5805–5811. (b) Kimura, E.; Shionoya, M.; Hoshino, A.; Ikeda, T.; Yamada, Y. *J. Am. Chem. Soc.* **1992**, 114, 10134–10137.

(7) (a) Koike, T.; Watanabe, T.; Aoki, S.; Kimura, E.; Shiro, M. *J. Am. Chem. Soc.* **1996**, 118, 12696–12703. (b) Kimura, E.; Koike, T. *Chem. Soc. Rev.* **1998**, 27, 179–184. (c) Kimura, E.; Aoki, S.; Kikuta, E.; Koike, T. *Proc. Natl. Acad. Sci. U.S.A.* **2003**, 100, 3731–3736. (d) Kimura, E.; Takasawa, R.; Tanuma, S.; Aoki, S. *Science STKE* **2004**, 223, 7.

(8) Aoki, S.; Kaido, S.; Fujioka, H.; Kimura, E. *Inorg. Chem.* **2003**, 42, 1023–1030.

(9) Aoki, S.; Kagata, D.; Shiro, M.; Takeda, K.; Kimura, E. *J. Am. Chem. Soc.* **2004**, 126, 13377–13390.

(10) Aoki, S.; Sakurama, K.; Matsuo, N.; Yamada, Y.; Takasawa, R.; Tanuma, S.; Shiro, M.; Takeda, K.; Kimura, E. *Chem.—Eur. J.* **2006**, 12, 9066–9080.

(11) Aoki, S.; Sakurama, K.; Ohshima, R.; Matsuo, N.; Yamada, Y.; Takasawa, R.; Tanuma, S.; Takeda, K.; Kimura, E. *Inorg. Chem.* **2008**, 47, 2747–2754.

(12) Pearce, D. A.; Jotterand, N.; Carrico, I. S.; Imperiali, B. *J. Am. Chem. Soc.* **2001**, 123, 5160–5161.

37.4, 46.1, 47.7, 49.9, 50.6, 54.3, 55.2, 58.1, 79.5, 125.9, 127.2, 128.5, 128.6, 128.8, 129.2, 132.0, 133.3, 134.0, 138.3, 142.0, 148.5, 155.7, 176.4 ppm. IR (KBr pellet): 2974, 2931, 2815, 1689, 1597, 1560, 1458, 1415, 1365, 1342, 1250, 1152, 1049, 962, 859, 774, 725, 622, 556 cm^{-1} . HRMS (FAB+): calcd for $[\text{M}+\text{H}]^+$, 984.3881; found, 984.3881.

1-[5,7-Bis(*N,N*-dimethylaminosulfonyl)-8-hydroxyquinolin-2-ylmethyl]-4,7,10-tris(*tert*-butyloxycarbonyl)-1,4,7,10-tetraazacyclododecane (17). One N aq. NaOH (1 mL) was added to a solution of **16** (80 mg, 0.081 mmol) in MeOH (5 mL) at room temperature, and the mixture was stirred at reflux temperature for 3 h. After cooling, the reaction mixture was concentrated under reduced pressure and purified by silica gel column chromatography ($\text{CH}_2\text{Cl}_2/\text{MeOH} = 100:1$) to afford **17** as a colorless powder (64 mg, 93% yield). mp. 95–98 °C. ^1H NMR (300 MHz, CDCl_3/TMS): δ 1.42–1.49 (m, 27H), 2.81 (s, 6H), 2.95 (s, 6H), 2.81–3.61 (m, 16H), 4.14 (s, 2H), 7.83 (d, $J = 9.0$ Hz, 1H), 8.50 (s, 1H), 9.02 ppm (d, $J = 9.0$ Hz, 1H). ^{13}C NMR (75 MHz, CDCl_3/TMS): δ 20.6, 22.6, 25.2, 28.4, 28.6, 31.5, 34.6, 37.4, 37.7, 47.4, 49.9, 54.5, 57.6, 79.7, 117.7, 122.9, 125.9, 126.3, 130.9, 134.8, 137.7, 154.6 ppm. IR (KBr pellet): 3447, 2974, 2931, 2815, 1689, 1597, 1560, 1458, 1415, 1365, 1250, 1152, 962, 859, 774, 725, 622, 556 cm^{-1} . HRMS (FAB–): calcd for $[\text{M}-\text{H}]^-$, 842.3792; found, 842.3793.

1-[5,7-Bis(*N,N*-dimethylaminosulfonyl)-8-hydroxyquinolin-2-ylmethyl]-1,4,7,10-tetraazacyclododecane Trihydrochloride Salt ($10 \cdot 3\text{HCl} \cdot \text{H}_2\text{O}$). Conc. HCl (1 mL) was added dropwise to a solution of **17** (290 mg, 0.34 mmol) in MeOH (5 mL), and the resulting solution was stirred at 70 °C for 10 min. The reaction mixture was concentrated under reduced pressure, azeotroped with CHCl_3 , and the resulting solid was recrystallized from $\text{H}_2\text{O}/\text{EtOH}$ to afford $10 \cdot 3\text{HCl}$ salt (characterized by elemental analysis and potentiometric pH titration) as a colorless powder (170 mg, 74% yield). After concentrating the filtrate under reduced pressure, a green powder was obtained, which was characterized as the $10 \cdot 4\text{HCl}$ salt (26 mg, 11% yield) by elemental analysis.¹⁵

For the $10 \cdot 3\text{HCl}$ salt: mp. > 250 °C. ^1H NMR (300 MHz, $\text{D}_2\text{O}/\text{external TSP}$): δ 2.81 (s, 6H), 2.89 (s, 6H), 3.05–3.25 (m, 16H), 4.22 (s, 2H), 7.75 (d, $J = 9.0$ Hz, 1H), 8.34 (s, 1H), 8.94 ppm (d, $J = 9.0$ Hz, 1H). ^{13}C NMR (75 MHz, $\text{D}_2\text{O}/\text{external 1,4-dioxane}$): δ 36.8, 37.2, 41.7, 42.5, 42.9, 48.6, 57.0, 115.4, 119.9, 126.5, 130.6, 135.4, 138.3, 156.5, 156.7 ppm. IR (KBr pellet): 3423, 2961, 1595, 1560, 1499, 1456, 1336, 1145, 1099, 1072, 955, 848, 787, 727, 622, 557 cm^{-1} . Elemental analysis: calcd for $\text{C}_{22}\text{H}_{42}\text{Cl}_3\text{N}_7\text{O}_6\text{S}_2$ (671.10): C, 39.37; H, 6.31; N, 14.61; found: C, 39.43; H, 6.39; N, 14.42.

For the $10 \cdot 4\text{HCl}$ salt: mp. 248–251 °C (decomp.). Elemental analysis: calcd for $\text{C}_{22}\text{H}_{41}\text{Cl}_4\text{N}_7\text{O}_5\text{S}_2$ (689.55): C, 38.32; H, 5.99; N, 14.22; found: C, 38.47; H, 6.28; N, 13.99.

1-[8-(Benzenesulfonyloxy)-5,7-bis(*N,N*-dimethylaminosulfonyl)quinolin-2-ylmethyl]-1,4,7,10-tetraazacyclododecane 3TFA Salt ($12 \cdot 3\text{TFA} \cdot 0.5\text{H}_2\text{O}$). A solution of trifluoroacetic acid (1.5 mL, 5.2 mmol) in CH_2Cl_2 (2.5 mL) was added to a solution of **16** (200 mg, 0.20 mmol) in CH_2Cl_2 (2.5 mL), and the resulting solution was stirred at 60 °C for 0.5 h. The reaction mixture was concentrated under reduced pressure, azeotroped with CHCl_3 , and the resulting residue was recrystallized from $\text{Et}_2\text{O}/\text{EtOH}$ to afford a $12 \cdot 3\text{TFA}$ salt ($12 \cdot 3\text{TFA} \cdot 0.5\text{H}_2\text{O}$) as a colorless powder (177 mg, 84% yield). mp. > 250 °C. ^1H NMR (300 MHz, $\text{D}_2\text{O}/\text{external TSP}$): δ 2.73 (s, 6H), 2.88 (s, 6H), 2.98–3.30 (m, 16H), 4.13 (s, 2H), 7.70 (t, $J = 7.8$ Hz, 2H), 7.89 (t, $J = 7.8$ Hz, 1H), 7.94–8.01 (m, 3H), 8.42 (s, 1H), 9.21 ppm (d, $J = 9.0$ Hz, 1H). ^{13}C NMR (75 MHz, $\text{D}_2\text{O}/\text{external 1,4-dioxane}$): δ 36.6,

36.8, 41.2, 41.6, 44.2, 47.7, 57.8, 126.8, 127.3, 127.7, 128.3, 129.1, 131.0, 134.5, 135.2, 135.4, 142.2, 147.6, 149.9, 159.8, 162.2, 162.6 ppm. IR (KBr pellet): 3411, 2923, 2851, 1682, 1550, 1454, 1347, 1202, 1142, 1071, 962, 835, 799, 722, 688, 607, 585, 556 cm^{-1} . Elemental analysis: calcd for $\text{C}_{34}\text{H}_{45}\text{F}_3\text{N}_7\text{O}_{13.5}\text{S}_3$ (1034.94): C, 39.46; H, 4.38; N, 9.47; found: C, 39.67; H, 4.63; N, 9.67.

1-[5,7-Bis(*N,N*-dimethylaminosulfonyl)-8-hydroxyquinolin-2-ylmethyl]-1,4,7,10-tetraazacyclododecane $\text{Zn}(\text{NO}_3)_2$ Complex ($11 \cdot \text{NO}_3 \cdot 1.3\text{H}_2\text{O}$). A solution of $\text{Zn}(\text{NO}_3)_2 \cdot 6\text{H}_2\text{O}$ (15 mg, 0.05 mmol) in water (1 mL) was added into a solution of $10 \cdot 3\text{HCl} \cdot \text{H}_2\text{O}$ (34 mg, 0.05 mmol) in H_2O (3 mL), and the pH of a reaction mixture adjusted to 10.0 by adding aq. NaOH. After the insoluble compounds were removed by filtration, the filtrate was slowly concentrated at atmospheric pressure to obtain $11 \cdot \text{NO}_3 \cdot 1.3\text{H}_2\text{O}$ as colorless prisms (8 mg, 23% yield). mp. > 250 °C. ^1H NMR (300 MHz, $\text{D}_2\text{O}/\text{external TSP}$): δ 2.74 (s, 6H), 2.86 (s, 6H), 2.91–3.20 (m, 16H), 4.34 (s, 2H), 7.74 (d, $J = 8.7$ Hz, 1H), 8.27 (s, 1H), 8.94 ppm (d, $J = 8.7$ Hz, 1H). ^{13}C NMR (75 MHz, DMSO/TMS): δ 37.0, 38.0, 43.6, 44.2, 45.0, 52.5, 57.5, 108.6, 116.0, 123.9, 126.7, 134.9, 136.8, 140.3, 155.4, 166.1 ppm. IR (KBr pellet): 3570, 3448, 3332, 3273, 2928, 2879, 1649, 1548, 1508, 1488, 1385, 1316, 1283, 1259, 1198, 1167, 1140, 1119, 1092, 1042, 993, 950, 930, 853, 796, 750, 720, 688, 596, 560 cm^{-1} . Elemental analysis: calcd for $\text{C}_{22}\text{H}_{36.6}\text{N}_8\text{O}_{9.3}\text{S}_2\text{Zn}$ (691.49): C, 38.21; H, 5.33; N, 16.20; found: C, 37.83; H, 5.21; N, 16.00.

Potentiometric pH Titrations. The preparation of the test solutions and the calibration method of the electrode system (Potentiometric Automatic Titrator AT-400 and Auto Piston Buret APB-410, Kyoto Electronics Manufacturing, Co. Ltd. with a Kyoto Electronics Manufacturing Co. Combination pH Electrode 98100C171) have been described in earlier reports.^{10,11} All test solutions (50 mL) were stored under an argon atmosphere. Potentiometric pH titrations were performed with $I = 0.1$ (NaNO_3) at 25 ± 0.1 °C. The deprotonation constants of Zn^{2+} -bound water $K_2' (= [\text{HO}^- \text{-bound species}][\text{H}^+]/[\text{H}_2\text{O-bound species}])$ were determined by means of the “BEST” software program.¹⁶ The K_w (equivalent to $a_{\text{H}^+}a_{\text{OH}^-}$), K_w' (equivalent to $[\text{H}^+][\text{HO}^-]$), f_{H^+} values used at 25 °C were $10^{-14.00}$, $10^{-13.79}$, and 0.825, respectively. The corresponding mixed constants $K_2 (= [\text{HO}^- \text{-bound species}]a_{\text{H}^+}/[\text{H}_2\text{O-bound species}])$, were derived by using $[\text{H}^+] = a_{\text{H}^+}/f_{\text{H}^+}$. The percentage species distribution values against pH ($= -\log [\text{H}^+] + 0.084$) were obtained using the SPE software program.¹⁶

Crystallographic Study of 10 ($\text{H}_2(\text{H}_{-1}\text{L}^6)$ ($= \text{HL}^6$)). **10** ($\text{H}_2(\text{H}_{-1}\text{L}^6)$ ($= \text{HL}^6$)) was recrystallized from an aqueous solution of **10** at pH 5 and 4 °C. These crystals, which were filtered and dried, were determined to be $[\text{HL}^6]^+ \cdot \text{Cl}^- \cdot 4.2\text{H}_2\text{O}$ by elemental analysis (Anal. Calcd for $\text{C}_{22}\text{H}_{38}\text{Cl}_1\text{N}_7\text{O}_{11.2}\text{S}_2 \cdot 4.2\text{H}_2\text{O}$: C 40.29, H 7.13, N 14.95. Found: C 39.85, H 6.68, N 14.61). All measurements were made on a Rigaku RAXIS-RAPID instrument with graphite monochromated Cu K α radiation at 93 K. The structure was solved by direct methods¹⁷ and refined by full-matrix least-squares techniques. All calculations were performed using the CrystalStructure crystallographic software package except for refinements, which were performed with SHELXL-97.¹⁸ $\text{C}_{22}\text{H}_{50.4}\text{Cl}_1\text{N}_7\text{O}_{11.2}\text{S}_2$, $M_r = 691.85$, a colorless block crystal, crystal size $0.15 \times 0.14 \times 0.14$ mm, monoclinic, space group $\text{C}2/c$ (#15), $a = 35.8779(7)$, $b = 19.7401(4)$, $c = 21.4880(7)$ Å, $\beta = 118.8100(7)^\circ$, $V = 13334.9(6)$ Å³, $Z = 16$, $D_{\text{calc}} = 1.378 \text{ g} \cdot \text{cm}^{-3}$, 91503 measured reflections, 11999 unique reflections, $2\theta_{\text{max}} = 68.3^\circ$, $R1$ ($wR2$) = 0.0685

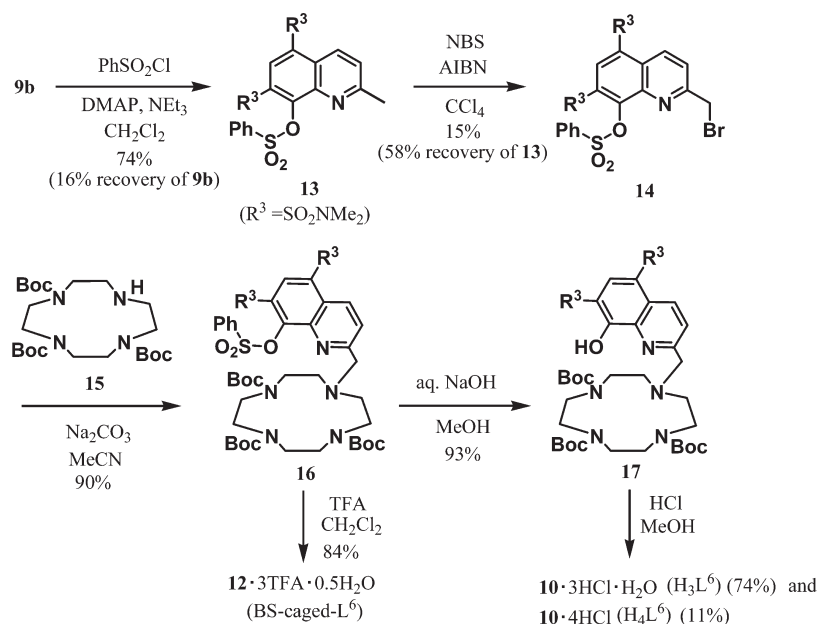
(16) Martell, A. E.; Motekaitis, R. J. *Determination and Use of Stability Constants*, 2nd ed.; VCH: New York, 1992.

(17) Burla, M. C.; Calandro, R.; Camalli, M.; Carrozzini, B.; Cascarano, G. L.; De Caro, L.; Giacovazzo, C.; Polidori, G.; Spagna, R. *J. Appl. Crystallogr.* **2005**, *38*, 381–388.

(18) Sheldrick, G. M. *SHELX-97, Program for the Refinement of Crystal Structures*; University of Göttingen: Göttingen, Germany, 1997.

(15) As described in the Experimental Section, 3HCl and 4HCl salt of **10** were obtained as colorless and green powders, respectively. As pointed out by the reviewer, this may be related to the protonation status of both salts in the solid state, although we do not have experimental evidence.

Scheme 4



(0.1966), GOF = 1.033. Full details of the crystallographic analysis of **10** are given in the Supporting Information.

Crystallographic Study of 11·NO₃ (Zn(H_{−1}L⁶)·NO₃). **11**·NO₃ (Zn(H_{−1}L⁶)·NO₃) was recrystallized by the slow evaporation of an aqueous solution. All measurements were made on a Rigaku Saturn CCD area detector with graphite monochromated Mo K α radiation at 133 K. C₂₂H₃₆N₈O₉S₂Zn, *M_r* = 686.07, a colorless block crystal, crystal size 0.25 × 0.20 × 0.15 mm, monoclinic, space group *P*2₁/*n* (#14), *a* = 11.602(5), *b* = 13.792(6), *c* = 17.941(8) Å, β = 93.923(3)°, *V* = 2864(2) Å³, *Z* = 4, *D_{calc}* = 1.591 g cm^{−3}, 22048 measured reflections, 7339 unique reflections, $2\theta_{\text{max}}$ = 57.4°, *R*1 (*wR*2) = 0.0646 (0.1901), GOF = 0.999. Full details of crystallographic analysis of **11**·NO₃ are given in the Supporting Information.

Photoreaction. Sample solutions were prepared in quartz cuvettes (GL Science Inc. Japan, 10 mm light path) and irradiated at a wavelength 328 or 330 nm on JASCO FP-6200 or those of FP-6500 spectrofluorometer. The photoreactions were followed by UV–vis (50 μ M) spectra or ¹H NMR spectra. The averaged light intensities of the JASCO FP-6200 spectrofluorometer at 330 nm were determined to be 1.4 × 10^{−5} mol·sec^{−1} (slit width for excitation = 20 nm), and those of the JASCO FP-6500 spectrofluorometer at 328 nm were determined to be 5.3 × 10^{−6} mol·sec^{−1} (slit width for excitation = 20 nm) relative to the potassium ferioxalate actinometer.¹³ The reactions were repeated two or three times, and the averaged values were calculated. Experimental fluctuations were \pm 5%.

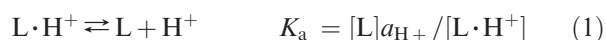
Treatment of HeLa Cells with Zn²⁺ Probes and Fluorescence Microscopy. HeLa cells were seeded onto 35 mm glass-bottom dishes. The cells were incubated with Zn²⁺ fluorophores **10** and **12** (50 μ M) in culture medium for 0.5 h in a humid atmosphere of 5% CO₂ at 37 °C, then washed twice with PBS, and the culture medium (2 mL) was replaced. The cells were treated with 25 μ M ZnSO₄·7H₂O and 20 μ M pyrithione for 10 min, washed with PBS and observed by phase contrast and fluorescence microscopy (KEYENCE fluorescent microscope, BZ-9000; excitation at 360/40 nm, emission 460/50 nm).

Results and Discussion

Synthesis of Zn²⁺ Fluorophores 10 and 12 (L⁶ and BS-caged-L⁶). A ligand **10** (L⁶) and its benzenesulfonyl-caged derivative **12** (BS-caged-L⁶) were synthesized as shown in

Scheme 4. The reaction of **9b**¹² with benzenesulfonyl chloride in the presence of 4-dimethylaminopyridine (DMAP) and Et₃N in CH₂Cl₂ gave **13**, the 2-methyl group of which was brominated with NBS and AIBN in CCl₄ to give **14**. The reaction of **14** with 3Boc-cyclen **15**¹⁴ gave **16**, the three Boc groups of which were deprotected with trifluoroacetic acid (TFA) in CH₂Cl₂ afforded **12** (BS-caged-L⁶) as the 3TFA salt. The PhSO₂ group of **16** was removed by treatment with aqueous NaOH to give **17**, the Boc groups of which were deprotected by treatment with HCl in MeOH afforded **10** (L⁶). It should be noted that **10** was obtained as a colorless powder, and concentration of its filtrate gave a green powder. These two powders were determined to be 3HCl salt (**10**·3HCl·H₂O) and 4HCl salt (**10**·4HCl), respectively, by elemental analysis and potentiometric pH titrations.¹⁵

Deprotonation Constants for 10 (L⁶) Determined by Potentiometric pH Titration, ¹H NMR, and UV–vis Spectra. A typical potentiometric pH titration curve for 1 mM **10**·3HCl·H₂O (H₃L⁶) + 2 mM HNO₃ against aqueous 0.1 M NaOH with *I* = 0.1 (NaNO₃) at 25 °C (dashed curve (a) in Figure 1) was analyzed for acid–base equilibrium (1). The deprotonation constants *pK_{ai}* (*i* = 1–6) of H₅L⁶ were determined to be < 2 (*pK_{a1}*~*pK_{a3}*), 2.5 \pm 0.1 (*pK_{a4}*), 9.7 \pm 0.1 (*pK_{a5}*), and 10.8 \pm 0.1 (*pK_{a6}*) (Table 1) by using the “BEST” software program.¹⁶ The *pK_{a1}*, *pK_{a2}*, *pK_{a5}*, and *pK_{a6}* values were assigned to the *pK_a* values for the four amines in the cyclen ring by comparison with the *pK_a* values for cyclen (L¹) and **5** (L⁵),¹⁰ as summarized in Table 1.



The deprotonation behavior of **10** is shown in Scheme 5. Changes in the UV–vis absorption of **10** at 265 nm in the pH range 1–4 (Figure S1a in the Supporting Information), gave a sigmoidal curve (a) with closed squares in Figure 2a, which gave a *pK_a* value of 2.7 \pm 0.2, suggesting that the *pK_{a2}* value of 2.5 determined by

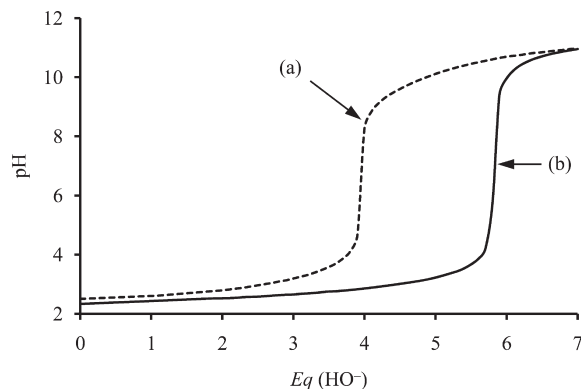


Figure 1. Typical potentiometric pH titration curves for (a) 1 mM H_3L^6 + 2 mM HNO_3 and (b) 1 mM H_3L^6 + 2 mM HNO_3 + 1 mM Zn^{2+} with $I = 0.1$ (NaNO_3) at 25 °C. $\text{Eq}(\text{HO}^-)$ is the number of equivalents of base (NaOH) added.

Table 1. Deprotonation Constants ($\text{p}K_{\text{a}}$) and Complexation Constants for Cyclen (L^1), **5** (L^5), and **10** (L^6) with Zn^{2+} in Aqueous Solution with $I = 0.1$ (NaNO_3) at 25 °C

	cyclen (L^1)	5 (L^5) ^a	10 (L^6)
$\text{p}K_{\text{a}1}$	<2	<2	<2
$\text{p}K_{\text{a}2}$	<2	<2	<2
$\text{p}K_{\text{a}3}$	9.9	<2	<2
$\text{p}K_{\text{a}4}$	11.0	7.2 ^b	2.51 ± 0.02^b $2.7 \pm 0.2^{b,c}$
$\text{p}K_{\text{a}5}$		10.1	9.69 ± 0.02
$\text{p}K_{\text{a}6}$		11.5	10.84 ± 0.02
$\log K_{\text{s}}(\text{ZnL})$	16.2	22.4	19.5
$\log K_{\text{app}}(\text{ZnL})$ at pH 7.4	10.6	14.1	13.3
$\log K_{\text{app}}(\text{ZnL})$ at pH 5.0	5.5	10.8	9.0

^a From ref 10. ^b The $\text{p}K_{\text{a}}$ values of 8-OH groups of quinolinol moieties. ^c The $\text{p}K_{\text{a}}$ value determined by pH-UV absorption profile.

potentiometric pH titration corresponds to the $\text{p}K_{\text{a}}$ value of the 8-OH group of **10** ($\text{H}_2\text{L}^6 \rightleftharpoons \text{H}_2(\text{H}_{-1}\text{L}^6)$ in Scheme 5). Interestingly, this value is much smaller than those for **5** (L^5) (7.0) and **9b** (6.1) (See also Scheme 3).

Figure 3a shows an ORTEP drawing for the single-crystal X-ray structure of $\text{H}_2(\text{H}_{-1}\text{L}^6)$ ($= \text{HL}^6$), in which the 8- O^- group of the quinolinolate moiety is hydrogen bonded to the ammonium cation of the cyclen ring. Representative crystallographic data for **10** (HL^6) and its Zn^{2+} complex **11** ($\text{Zn}(\text{H}_{-1}\text{L}^6)$) displayed below are listed in Table 2. A space-filling model of the same crystal (Figure 3b) suggests that the 8- O^- group of quinolinolate (O1 in Figure 3b) is surrounded by the quinoline ring, the Me_2NSO_2 group at the 7-position of 8-quinolinolate, and the cyclen ring. We, therefore, consider that the ion pair of $\text{Ar}-\text{O}^-$ (quinolinolate) and the ammonium group (cyclen ring) is stabilized in this hydrophobic space, resulting in the extremely lower $\text{p}K_{\text{a}}$ value of 2.5 in the ground state, compared to that for **9b** (6.1).¹⁹

pH-Dependent Fluorescent Behaviors of **10 (L^6).** The pH-emission profile of **10** (excitation at 370 nm and emission at 478 nm) in Figure 2 (closed circles) shows a sigmoidal curve giving a $\text{p}K_{\text{a}}$ value of around 10–11 (See

also Figure S1b in the Supporting Information). This $\text{p}K_{\text{a}}$ value obtained from emission spectra is much greater than the $\text{p}K_{\text{a}}$ value of 2.5–2.7 in the ground state determined by potentiometric pH and UV–vis titrations. For comparison, the emission intensity of **9b** is very small in the pH range of 2–13, as indicated by the open circles (c) in Figure 2. Therefore, this unique emission behavior of **10** can be attributed to the effect of its cyclen ring. Moreover, UV–vis absorption spectra of **10** at pH 10–12 showed negligible change, as displayed in Figure 2 and Figure S1 in the Supporting Information, supporting that the $\text{p}K_{\text{a}}$ value of around 10–11 obtained from pH–emission profile (Figure 2) corresponds to the $\text{p}K_{\text{a}}$ value of quinolinol group in **10** influenced by the cyclen ring in the excited state. We previously observed a similar phenomenon for **5** (L^5) and concluded that fluorescent quenching of quinolinols, which resulted in the higher $\text{p}K_{\text{a}}$ value obtained from emission spectra than that in the ground state, was due to the excited-state proton transfer (ESPT) from the cyclen ring.²⁰ Analogously, in the case of the anionic quinolinolate of the $\text{H}_2(\text{H}_{-1}\text{L}^6)$ ($= \text{HL}^6$) form or the $\text{H}(\text{H}_{-1}\text{L}^6)$ ($= \text{L}^6$) form, we assume that protons would be extracted from the protonated cyclen ring (its higher two $\text{p}K_{\text{a}}$ values, $\text{p}K_{\text{a}5}$ and $\text{p}K_{\text{a}6}$, are 9.7 and 10.8, respectively) in the excited states (Scheme 5), resulting in the quenching of its fluorescent emission.²¹

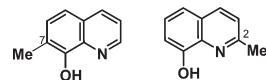
UV–vis and Emission Titrations of **10 (L^6) with Zn^{2+} .** Figure 4a shows the results of the UV–vis absorption titration of 50 μM **10** (L^6) with Zn^{2+} at pH 7.4 (10 mM HEPES with $I = 0.1$ (NaNO_3)) and 25 °C. The absorption maximum shifted from 265 to 269 nm upon addition of the Zn^{2+} (0–1.0 equiv) with isosbestic points at 284 and 370 nm.

As shown in Figure 4b, the emission of **10** (5 μM) was very weak at pH 7.4 and quantitatively increased with increasing Zn^{2+} concentrations (excitation at 370 nm, which is an isosbestic point found in Figure 4a), reaching a plateau at 1.0 equiv with 32-fold increase in emission intensity at 478 nm (the inset of Figure 2b), which strongly indicated a 1:1 complexation of **10** with Zn^{2+} , considering together with the results of UV–vis titration.

Figure 5 shows a comparison of the pH-dependent changes in emission intensity of the two Zn^{2+} complexes, **6** and **11** (5 μM). It is noteworthy that the fluorescent emission of **11** ($\text{Zn}(\text{H}_{-1}\text{L}^6)$, $\Phi_{\text{F}} = 0.41$ at pH 7.4) is much greater than that of **6** ($\text{Zn}(\text{H}_{-1}\text{L}^5)$, $\Phi_{\text{F}} = 0.044$ at pH 7.4), indicating that **10** is a more sensitive Zn^{2+} probe than L^5 . The facts that emission of **11** is almost constant at pH 4–11 and that the emission of **10** is very weak below pH 9

(20) (a) Bardez, E.; Chatelain, A.; Larrey, B.; Valeur, B. *J. Phys. Chem.* **1994**, *98*, 2357–2366. (b) Bardez, E.; Devol, I.; Larrey, B.; Valeur, B. *J. Phys. Chem. B* **1997**, *101*, 7786–7793. (c) Cheatum, C. M.; Heckscher, M. M.; Crim, F. F. *Chem. Phys. Lett.* **2001**, *349*, 37–42. (d) Li, Q.-S.; Fang, W.-H. *Chem. Phys. Lett.* **2003**, *367*, 637–644.

(21) Prodi, Izatt, and Savage et al. reported that the fluorescent emission intensity of 7-methyl-8-quinolinol was much greater than that of 2-methyl-8-quinolinol, suggesting that a functional group at the 7-position affects the photochemical properties of 8-quinolinols. Bronson, R. T.; Montalti, M.; Prodi, L.; Zaccaroni, N.; Lamb, R. D.; Dalley, N. K.; Izatt, R. M.; Bradshaw, J. S.; Savage, P. B. *Tetrahedron* **2004**, *60*, 11139–11144.



(19) As shown in Figure S2 in the Supporting Information, $\text{H}_2(\text{H}_{-1}\text{L}^6)$ was isolated as a dimeric structure. We cannot exclude the possibility that π – π interactions between two quinolinol moieties from two separate molecules of L^6 could facilitate the deprotonation of the 8-OH groups.

(Figures 2 and 4b) would permit a quantitative measurement of Zn^{2+} to be made at pH 4–9.

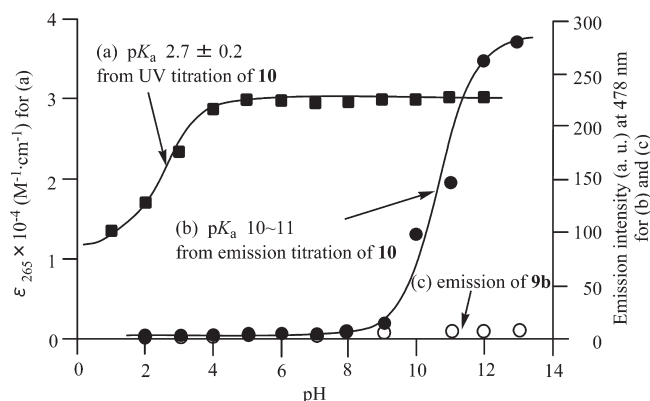


Figure 2. pH-dependent change in ϵ_{265} (a) (closed squares) and emission intensity at 478 nm (b) (closed circles) for **10** (L^6) (excitation at 370 nm). $[\mathbf{10}] = 50 \mu\text{M}$ for UV-vis spectra and $5 \mu\text{M}$ for emission spectra in comparison with that of $5 \mu\text{M}$ **9b** at 478 nm (c, open circles).

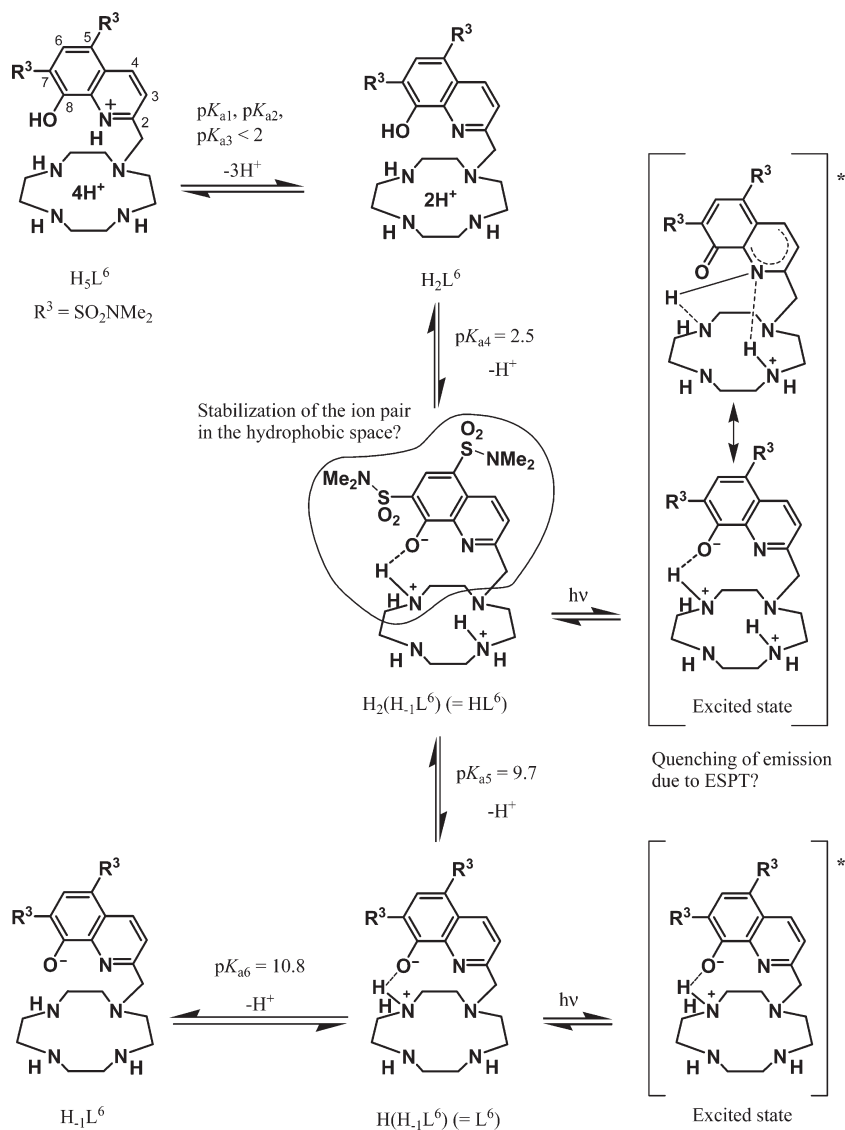
Complexation Behavior of $\mathbf{10}$ (L^6) with Zn^{2+} As Studied by Potentiometric pH Titrations. Analysis of a potentiometric pH titration curve for a mixture of 1 mM H_3L^6 , 2 mM HNO_3 , and 1 mM ZnSO_4 (curve b in Figure 1) with the “BEST” software program¹⁶ gave a complexation constant defined by eq 2, $\log K_s(\text{Zn}(\text{H}_{-1}\text{L}^6))$, of 19.5, from which the apparent complexation constants, $\log K_{\text{app}}(\text{Zn}(\text{H}_{-1}\text{L}^6))$, were calculated to be 13.3 at pH 7.4 (dissociation constant, K_d , is 50 fM) and 9.0 at pH 5.0, respectively (See also Table 1). The $K_s(\text{Zn}(\text{H}_{-1}\text{L}^6))$ value for **11** is slightly smaller than that for **6**, possibly because of the electron-withdrawing effect of the SO_2NMe_2 at the 7-position. Figure 6 shows a distribution diagram for a mixture of $5 \mu\text{M}$ **10** (L^6) and $5 \mu\text{M}$ Zn^{2+} obtained by calculation using the software program “SPE”,¹⁶ indicating that $\text{Zn}(\text{H}_{-1}\text{L}^6)$ is quantitatively formed at $\text{pH} > 5$ in micromolar concentrations.

$$K_s(\text{Zn}(\text{H}_{-1}\text{L})) = [\text{Zn}(\text{H}_{-1}\text{L})]/[\text{H}_{-1}\text{L}][\text{Zn}^{2+}] \quad (2)$$

$$K_{\text{app}}(\text{Zn}(\text{H}_{-1}\text{L})) = [\text{Zn}(\text{H}_{-1}\text{L})]/[\text{L}]_{\text{free}}[\text{Zn}^{2+}]_{\text{free}} \quad (3)$$

$$[\text{L}]_{\text{free}} = \sum [\text{H}_n\text{L}]_{\text{free}} \text{ at designated pH } (n = (-1) \sim 5) \quad (4)$$

Scheme 5



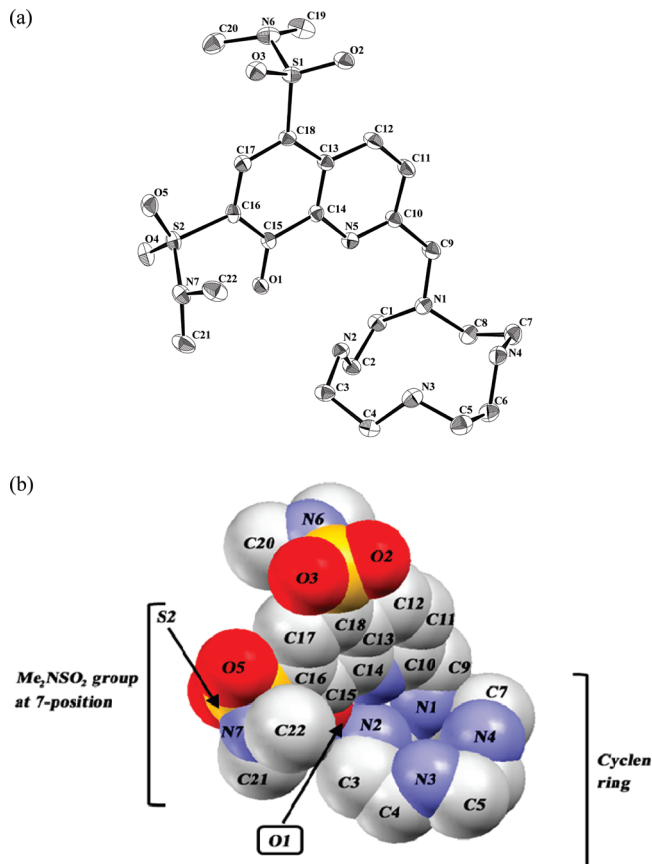


Figure 3. (a) ORTEP drawing (50% probability ellipsoids) of **10** ($\text{H}_2(\text{H}_{-1}\text{L}^6)$) ($= \text{HL}^6$). Selected bond lengths [Å]: O(1)–C(15) 1.272(4), S(2)–C(16) 1.756(3), S(2)–N(7) 1.629(3), N(7)–C(22) 1.476(5), N(7)–C(21) 1.472(5). Water, hydrogen chloride and hydrogen atoms have been omitted for clarity. (b) Space-filling model of **10** ($\text{H}_2(\text{H}_{-1}\text{L}^6)$) ($= \text{HL}^6$). The crystallographic parameters are given in Table 2.

Table 2. Crystallographic Data for **10** ($\text{H}_2(\text{H}_{-1}\text{L}^6)$) ($= \text{HL}^6$) and **11** ($\text{Zn}(\text{H}_{-1}\text{L}^6)$)

	10 ($\text{H}_2(\text{H}_{-1}\text{L}^6)$) ($= \text{HL}^6$)	11 ($\text{Zn}(\text{H}_{-1}\text{L}^6)$)
chemical formula	$\text{C}_{22}\text{H}_{50.4}\text{Cl}_1\text{N}_7\text{O}_{11.2}\text{S}_2$	$\text{C}_{22}\text{H}_{36}\text{N}_8\text{O}_9\text{S}_2\text{Zn}_1$
formula weight	691.85	686.07
space group	$C2/c$ (#15)	$P2_1/n$ (#14)
a (Å)	35.8779(7)	11.602(5)
b (Å)	19.7401(4)	13.792(6)
c (Å)	21.4880(7)	17.941(8)
β (deg)	118.8100(7)	93.923(3)
V (Å ³)	13334.9(6)	2864(2)
Z	16	4
T (°C)	−180	−140
λ (Å)	1.54187	0.71070
D_{calc} (g·cm ^{−3})	1.378	1.591
μ (Cu K α for 10 and Mo K α for 11) (cm ^{−1})	27.38	10.68
$R1$ ($I > 2\sigma(I)$)	0.0685	0.0646
$wR2$ (all reflections)	0.1966	0.1901

X-ray Crystal Structure of **11 ($\text{Zn}(\text{H}_{-1}\text{L}^6) \cdot \text{NO}_3 \cdot \text{H}_2\text{O}$).** Colorless crystals were obtained from a 1:1 mixture of **10** (L^6) and Zn^{2+} in aqueous solution at pH 10. A single-crystal X-ray structure analysis disclosed that the Zn^{2+} in **11** (Figure 7) is six-coordinated by the deprotonated O(1) at the 8-position of the quinoline ring, N(5) of the quinoline ring, and N(1)–N(4) of the cyclen ring, similar to the previously reported Zn^{2+} complex **6**.¹⁰ The bond lengths of Zn(1)–O(1), Zn(1)–N(1), Zn(1)–N(3), and Zn(1)–N(5)

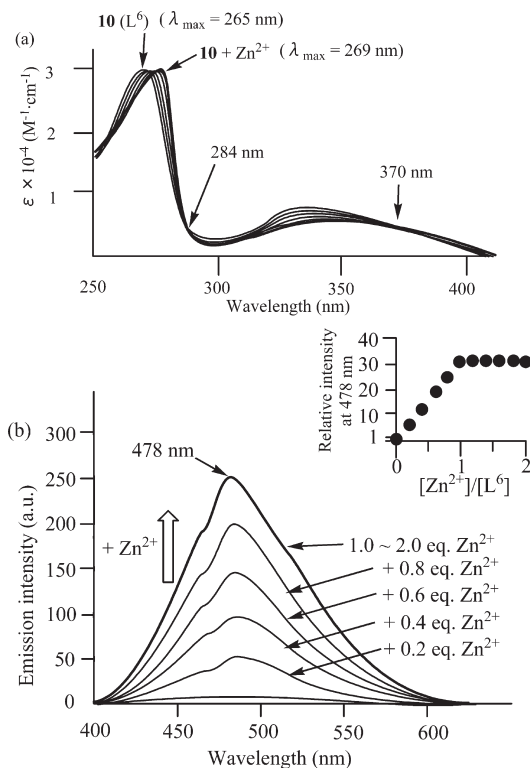


Figure 4. (a) Change in UV–vis spectra of $50 \mu\text{M}$ **10** (L^6) with Zn^{2+} (0–2.0 equiv), pH 7.4 (10 mM HEPES) with $I = 0.1$ (NaNO_3) at 25°C . (b) Change in the emission spectra of $5 \mu\text{M}$ **10** (L^6) with Zn^{2+} (0–2.0 equiv), pH 7.4 with $I = 0.1$ (NaNO_3) at 25°C (excitation at 370 nm). The inset shows the increase in the relative emission intensity of **10** (L^6) at 478 nm on the addition of Zn^{2+} .

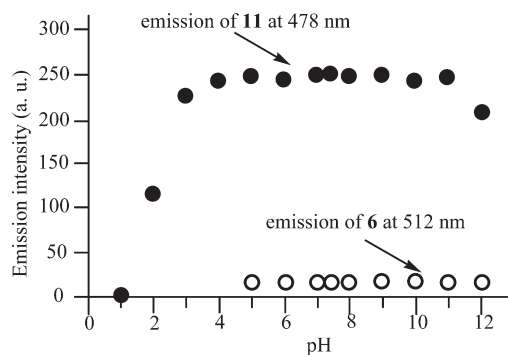


Figure 5. pH-Dependent change in the emission intensity of **6** ($\text{Zn}(\text{H}_{-1}\text{L}^5)$) (open circles) and **11** ($\text{Zn}(\text{H}_{-1}\text{L}^6)$) (closed circles) with $I = 0.1$ (NaNO_3) at 25°C (excitation at 338 nm for **6** and at 370 nm for **11**, $[\text{6}] = [\text{11}] = 5 \mu\text{M}$). Arbitrary unit is a.u.

are 2.10–2.13 Å, which are shorter than Zn(1)–N(2) and Zn(1)–N(4). Four N atoms of the cyclen ring and the Zn^{2+} ion form a tetragonal-pyramidal structure. Representative crystallographic parameters of **11** are listed in Table 2.

Fluorescent Response of **10 to Various Metal Ions.** We examined the fluorescent response of **10** ($5 \mu\text{M}$) to various metal ions in aqueous solutions at pH 7.4. As shown in Figure 8, **10** shows selectivity of fluorescent response to Zn^{2+} (32 times emission enhancement) and Cd^{2+} (41 times enhancement). When Cu^{2+} , Co^{2+} , Mn^{2+} , or Fe^{2+} were added to **10** prior to the addition of Zn^{2+} , the increase in emission was inhibited. The results of UV–vis

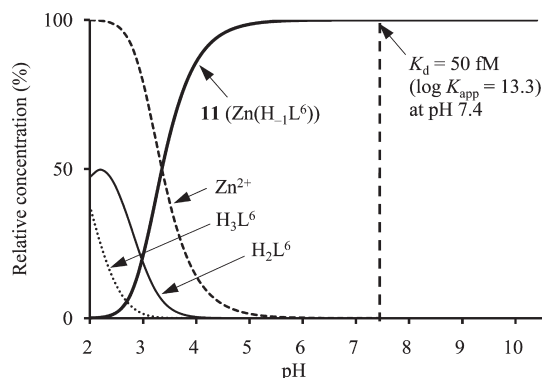


Figure 6. Distribution diagram for a mixture of $5\ \mu\text{M}$ **10** (L^6) + $5\ \mu\text{M}$ Zn^{2+} with $I = 0.1$ (NaNO_3) at $25\ ^\circ\text{C}$.

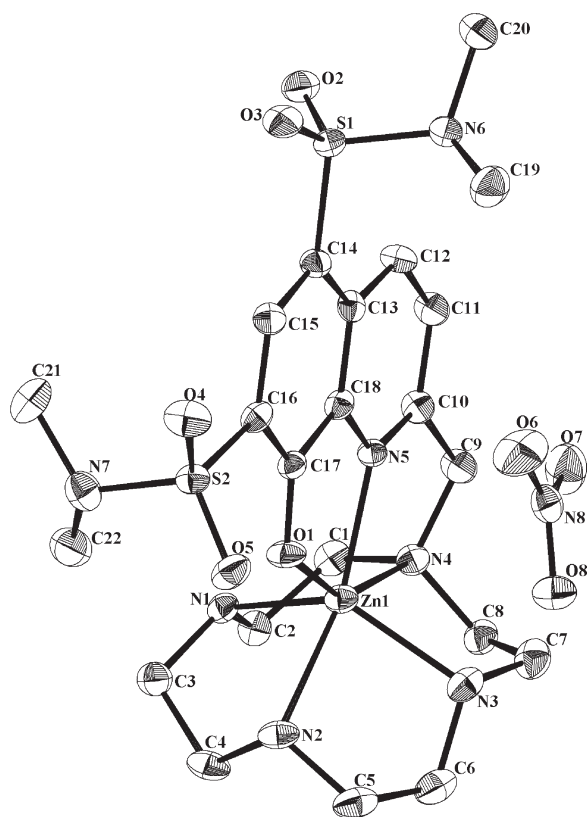


Figure 7. ORTEP drawing (50% probability ellipsoids) of **11** ($\text{Zn}(\text{H}_{-1}\text{L}^6)$). Selected bond lengths [\AA]: $\text{Zn}(1)\text{--O}(1)$ 2.123(2), $\text{Zn}(1)\text{--N}(1)$ 2.129(3), $\text{Zn}(1)\text{--N}(2)$ 2.229(3), $\text{Zn}(1)\text{--N}(3)$ 2.126(3), $\text{Zn}(1)\text{--N}(4)$ 2.427, $\text{Zn}(1)\text{--N}(5)$ 2.103(3). Water and hydrogen atoms have been omitted for clarity.

titrations of **10** with Cu^{2+} , Mn^{2+} , Co^{2+} , and Fe^{2+} suggested that **10** forms 1:1 complexes with these metal cations as shown in Figure S3 and S4 in the Supporting Information (the $\log K_{\text{app}}$ values were estimated to be $> 10^8$ for Cu^{2+} , Co^{2+} , and Mn^{2+} , and $> 10^6$ for Fe^{2+}).²² Therefore, the inhibition of the emission by these metal cations could be attributed to competitive binding with Zn^{2+} for **10** and/or quenching of the emission by paramagnetic metal cations.²³

(22) The apparent complexation of **10** with Fe^{2+} may be underestimated because of the UV-vis absorption of Fe^{2+} itself at 250–600 nm.

(23) Lu, C.; Xu, Z.; Cui, J.; Zhang, R.; Qian, X. *J. Org. Chem.* **2007**, *72*, 3554–3557.

Zn^{2+} -Dependent Hydrolytic Uncaging of **12.** As described in the Introduction, we reported on the synthesis of a benzenesulfonyl-caged (BS-caged) derivative of L^5 (**7**) in our previous report.¹¹ We then synthesized **12** in this study (Scheme 3) and tested Zn^{2+} -promoted hydrolytic uncaging, as evidenced by changes in UV-vis absorption spectra (Figure 9). While **12** was resistant to hydrolysis in the absence of Zn^{2+} at pH 7.4, the addition of Zn^{2+} triggered the increase in UV absorption at 269 nm with isosbestic points at 249, 281, and 329 nm, strongly suggesting the hydrolytic removal of the benzenesulfonyl moiety of **12** by Zn-bound HO^- to give **11** ($\text{Zn}(\text{H}_{-1}\text{L}^6)$), as shown in Scheme 3. The Zn^{2+} -dependent hydrolysis of **12** was also confirmed by ^1H NMR and UV-vis spectra measurements (Figures S5 and S6 in the Supporting Information).

Supporting Information, Figure S7 shows the time course for the hydrolysis of **12** at pH 5–9, from which the linear rate constants, k_1 (sec^{-1}), at pH 5.0, 6.0, 7.0, 7.4, 8.0, and 9.0 were determined and plotted in Figure 10a. The k_1 -pH profiles for **12** gave a kinetic pK_a value of 7.7 ± 0.2 , which is in good agreement with the kinetic pK_a values of 7.7 for **7**,¹¹ suggesting that the hydrolysis of **12** is promoted by Zn-bound HO^- . The data shown in figure 10a also indicates that the hydrolysis rate of **12** was much greater than that of **7** because of the electron-withdrawing effect of the SO_2NMe_2 group at the 7-position.

From an Eyring plot (the $1/T\text{--}\ln(k/T)$ profile in Figure 10b) for the hydrolytic uncaging of **12** (BS-caged- L^6) promoted by Zn^{2+} or Cd^{2+} -bound HO^- , the Gibbs activation energy, ΔG^\ddagger , the enthalpy of activation, ΔH^\ddagger , and the entropy of activation, ΔS^\ddagger , were calculated and the results were summarized in Table 3. The $(-T\Delta S^\ddagger)$ values for the hydrolysis of **12** with Zn^{2+} and Cd^{2+} are nearly zero. We presume that hydrophobic and steric effect of the Me_2NSO_2 group at the 7-position of the quinoline moiety fix the conformation of the PhSO_2 group and hence restrict the transition states of the Zn^{2+} and Cd^{2+} -promoted hydrolysis, resulting in negligible change in the degree of freedom (**18a** and **18b** in Scheme 6). The smaller ΔH^\ddagger value for the Cd^{2+} -promoted hydrolysis of **12** than that for the Zn^{2+} -promoted hydrolysis indicates the possibility of a different mechanism operating in these two reactions. The Cd^{2+} ion, which has a larger ionic radius than that of Zn^{2+} , might be coordinated by the PhSO_2 moiety, resulting in a higher reactivity of the PhSO_2 group in **18** (Scheme 6).

Measurement of Zn^{2+} Concentrations in Sample Solutions by **12 (BS-caged- L^6).** We attempted to quantitatively measure $[\text{Zn}^{2+}]$ in some sample solutions utilizing **12**. Essentially no change in the emission of **12** was observed in the absence of Zn^{2+} , as mentioned above, and the addition of given amounts of Zn^{2+} ($0\text{--}5\ \mu\text{M}$) followed by incubation at $25\ ^\circ\text{C}$ for 30 min induced a nearly linear increase in emission, as shown in Figure S8 in the Supporting Information and Figure 11. In addition, it was found that this hydrolysis reaction of **12** with Zn^{2+} completes within 10 min at $50\ ^\circ\text{C}$ (Figure S6 in the Supporting Information), indicating that **12** has considerable potential for use in the quantitative analysis of Zn^{2+} in solutions.

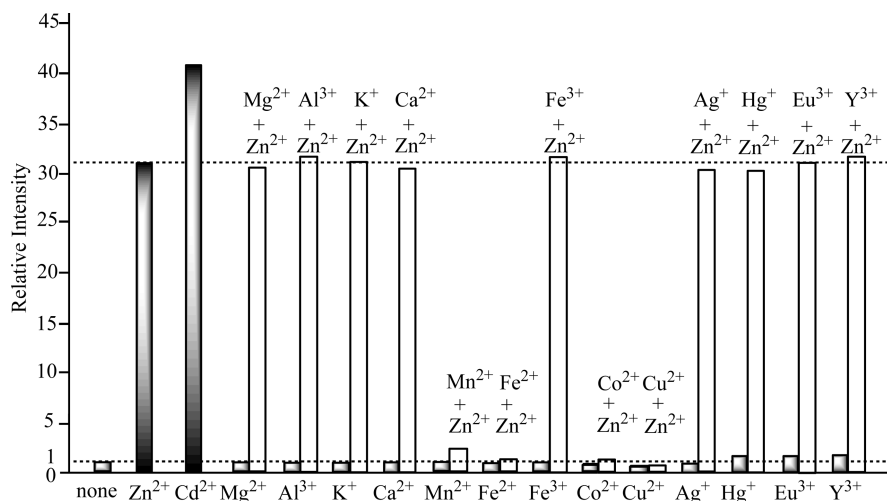


Figure 8. Fluorescent response of $5 \mu\text{M}$ **10** (L^6) at 478 nm to 1.0 equiv of various metal cations (shaded bars) and to 1.0 equiv of Zn^{2+} added after 1.0 equiv of various metals (open bars) at $\text{pH } 7.4$ (10 mM HEPES) with $I = 0.1$ (NaNO_3) at 25°C .

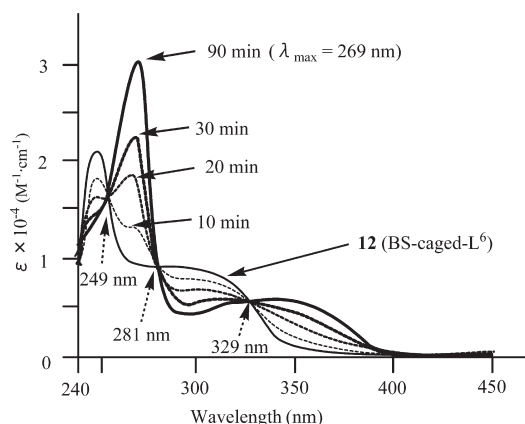


Figure 9. Change in UV-vis spectra as the result of the Zn^{2+} -promoted hydrolysis of $50 \mu\text{M}$ **12** (BS-caged- L^6) in the presence of $50 \mu\text{M}$ Zn^{2+} at $\text{pH } 7.4$ (10 mM HEPES) with $I = 0.1$ (NaNO_3) at 37°C .

Metal Selectivity in the Hydrolytic Uncaging of **12 (BS-caged- L^6).** We examined the hydrolytic uncaging of **12** ($50 \mu\text{M}$) in the presence of Cd^{2+} , Cu^{2+} , Mn^{2+} , Co^{2+} , Fe^{2+} , Fe^{3+} , Ca^{2+} , and Mg^{2+} ($50 \mu\text{M}$ each) at $\text{pH } 7.4$ at 25°C , as evidenced by changes in UV-vis absorption spectra like Figure 9. We previously reported that the Cd^{2+} -catalyzed hydrolysis of **7** proceeds at almost same speed as Zn^{2+} -catalyzed hydrolysis.¹¹ Concerning **12**, hydrolysis by Cd^{2+} was faster than that by Zn^{2+} . The ϵ_{269} values increased in the presence of Cu^{2+} , Mn^{2+} , Co^{2+} , and Fe^{2+} , indicating that these metals promoted a partial hydrolysis of **12** (data not shown). The ϵ_{269} value decreased with Fe^{3+} , possibly because of the complexation of **12** with Fe^{3+} without hydrolysis.

Photochemical Uncaging of **12 (BS-caged- L^6).** In our previous paper,¹¹ we reported that the benzenesulfonyl moiety of **7** can be removed by photoirradiation in aqueous solution to give **5** and benzenesulfonate (Scheme 2). Thus, we examined the photoreaction of **12**, as followed by UV-vis (Figure 12) and ^1H NMR (Figure S9 in the Supporting Information) spectra. The UV-vis absorption curve for **12** ($50 \mu\text{M}$, curve (a) in Figure 12) changed to curve (b) after photoirradiation at 330 nm for

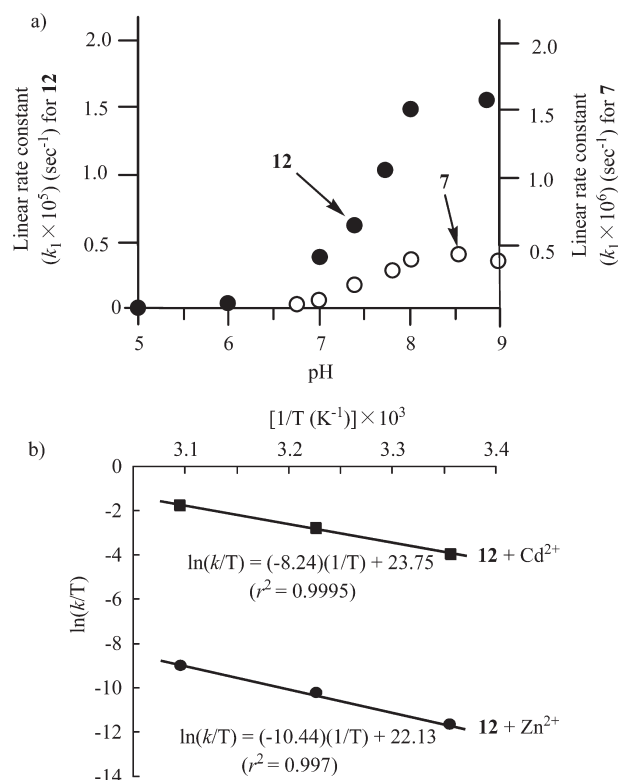
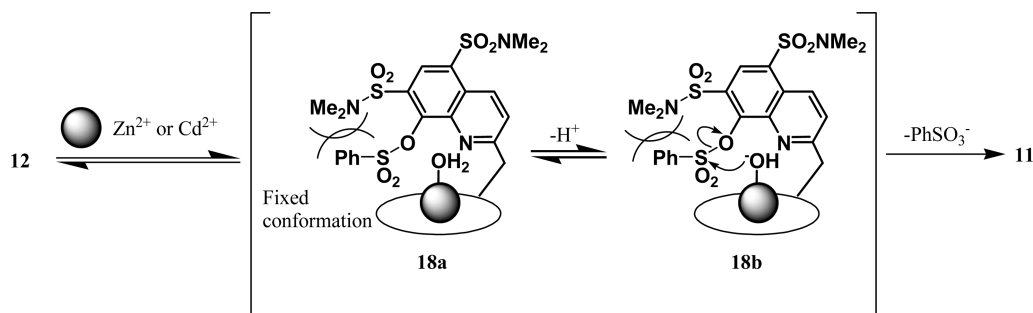


Figure 10. (a) pH-dependent plot of linear rate constants for the hydrolytic uncaging of **7** (BS-caged- L^5) and **12** (BS-caged- L^6) in the presence of Zn^{2+} at 25°C . (b) $1/T - \ln(k/T)$ profile for the hydrolytic uncaging of **12** (BS-caged- L^6) promoted by Zn^{2+} or Cd^{2+} -bound HO^- ($[\text{12}] = [\text{Zn}^{2+}] = [\text{Cd}^{2+}] = 50 \mu\text{M}$ in 10 mM HEPES ($\text{pH } 7.4$) with $I = 0.1$ (NaNO_3)).

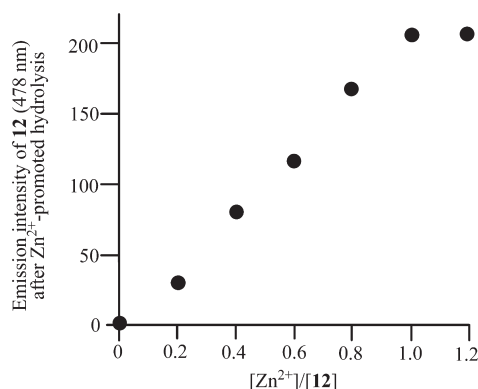
10 min in the absence of Zn^{2+} . Photoirradiation for 30 min gave curve (c), which agreed well with that of **10** (not shown). The fact that curves (a), (b), and (c) have an isosbestic point at 322 nm suggests that photolysis of **12** affords two main products **10** (L^6) and benzenesulfonate (PhSO_3^-), as proven by ^1H NMR experiments (described below). Another isosbestic point at about 280 nm is not so clear, possibly because of the formation of PhSO_3^- that

Scheme 6

**Table 3.** Comparison of Activation Parameters for Hydrolysis of **7** and **12** Promoted by Zn^{2+} or Cd^{2+} -bound HO^- (pH 7.4 with $I = 0.1$ (NaNO_3))^a

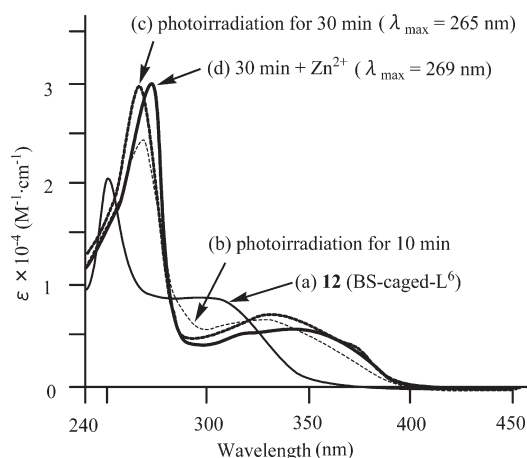
ligands	metals	ΔG^\ddagger (kcal/mol)	ΔH^\ddagger (kcal/mol)	$-T\Delta S^\ddagger$ (kcal/mol) ^b
7	Zn^{2+}	24 ^c	19 ^c	4.6 ^c
7	Cd^{2+}	19 ^c	20 ^c	-0.6 ^c
12	Zn^{2+}	21	21	0.2
12	Cd^{2+}	16	16	0.0

^a $[\text{7}] = [\text{12}] = [\text{Zn}^{2+} \text{ or } \text{Cd}^{2+}] = 50 \mu\text{M}$. ^b $T = 298 \text{ K}$. ^c From ref 11.

**Figure 11.** Quantitative increase in the fluorescent intensity of $5 \mu\text{M}$ **12** (BS-caged- L^6) by Zn^{2+} -dependent hydrolysis ($[\text{Zn}^{2+}] = 0\text{--}6 \mu\text{M}$) (emission was observed 478 nm with excitation at 370 nm) at pH 7.4 (10 mM HEPES with $I = 0.1$ (NaNO_3)) and 37°C (see also Figure S8 in the Supporting Information). Emission spectra were obtained by rapidly scanning the emission wavelength, to minimize photochemical uncaging (See below).

has small absorption at 240–290 nm ($\epsilon_{260} \approx 0.6 \times 10^4 \text{ M}^{-1}\cdot\text{cm}^{-1}$). The addition of 1.0 equiv of Zn^{2+} to curve (c) gave curve (d) with an absorption maximum at 269 nm, strongly suggesting the formation of **10** ($\text{Zn}(\text{H-L}^6)$). The quantum yield for the photolysis of **12** ($500 \mu\text{M}$) was calculated to be 7.2×10^{-5} , which was greater than that of **7** (2.3×10^{-5}).¹¹

The photolysis of **12** (1 mM) in D_2O at pD 7.4 was also confirmed by ^1H NMR experiments. After photoreactions for 30 and 90 min (irradiation at 330 nm), the spectra changed to those shown in Figures S9b and S9c in the Supporting Information, in which new ^1H signals appeared, showing good coincidence with those of **10** (L^6) (Figure S9d in the Supporting Information) and PhSO_3^- . Upon the addition of Zn^{2+} to the solution shown in Figure S9c, Figure S9e was obtained, indicating the formation of **11** (Figure S9f). It is also noteworthy that the photolysis proceeded quantitatively with negligible byproducts being produced in aqueous solution. Our

**Figure 12.** Photolysis of $50 \mu\text{M}$ **12** in pH 7.4 (10 mM HEPES with $I = 0.1$ (NaNO_3)) at 25°C (photoirradiation at 330 nm) followed by UV-vis absorption spectra. After 30 min of irradiation, 1.0 equiv of Zn^{2+} was added into the reaction mixture.

recent study on the reaction mechanism involved in the photolysis of **7** (BS-caged- L^5), **12** (BS-caged- L^6), and some 8-quinolynyl sulfonate derivatives that have no cyclen unit suggested that this photolysis proceeds via homolytic S–O bond fission in the excited triplet state.²⁴

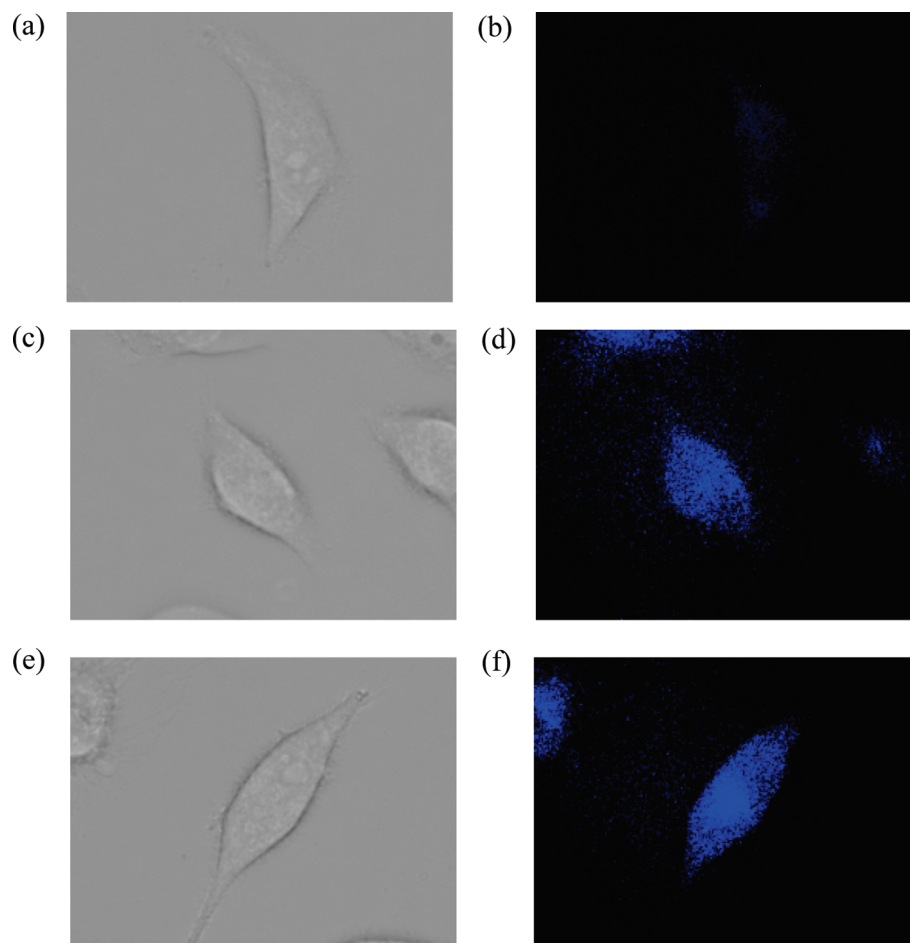
Comparison of Intracellular Concentrations of Zn^{2+} Probes. Intracellular concentrations of **2** (L^2), **5** (L^5), **10** (L^6), and **12** (BS-caged- L^6) in HeLa cells were estimated using our previously developed methods (concentrations of these probes: $50 \mu\text{M}$, culture time: 0.5–1.0 h at 37°C).¹¹ As summarized in Table 4, the intracellular concentration of **12** ($10 \pm 1 \mu\text{M}$) was higher than **10** ($2 \pm 1 \mu\text{M}$), possibly because of the presence of the two Me_2NSO_2 groups. Negligible cell damage was observed under these culture conditions.

Fluorescent Staining of Zn^{2+} -loaded HeLa Cells. Cell staining experiments of Zn^{2+} in HeLa cells were performed using **10** and **12**. Figures 13a and 13b show phase contrast and fluorescent images of HeLa cells treated with $50 \mu\text{M}$ **10**. Figures 13c and 13d show data treated with $50 \mu\text{M}$ **10** for 0.5 h and then $25 \mu\text{M}$ ZnSO_4 and $20 \mu\text{M}$ Zn^{2+} pyrrithione (Zn^{2+} carriers). Figures 13e and 13f show images of cells that had been treated with $50 \mu\text{M}$ **12** for 0.5 h and then $25 \mu\text{M}$ ZnSO_4 and $20 \mu\text{M}$ Zn^{2+} pyrrithione. These results indicate that **10** and **12** would be useful for detecting levels of intracellular Zn^{2+} .

(24) Kageyama, Y.; Ohshima, R.; Sakurama, K.; Fujiwara, Y.; Tanimoto, Y.; Yamada, Y.; Aoki, S. *Chem. Pharm. Bull.* **2009**, *57*, 1257–1266.

Table 4. Estimated Intracellular Concentrations of Zn^{2+} Fluorophores in HeLa Cells

	2 (L^2)	5 (L^5)	7 (BS-caged- L^5)	10 (L^6)	12 (BS-caged- L^6)
intracellular concentrations (μM)	8 ± 1^a	0^a	12 ± 3^a	2 ± 1	10 ± 2

^a From ref 11.**Figure 13.** Microscopic images ($\times 60$ with digital zoom ($\times 3.0$)) of HeLa cells stained with $50 \mu\text{M}$ **10** without Zn^{2+} -pyrithione (a: phase contrast, b: fluorescent) and **10** (c: phase contrast, d: fluorescent) and **12** (e: phase contrast, f: fluorescent) with $25 \mu\text{M}$ ZnSO_4 and $20 \mu\text{M}$ pyrithione.

Conclusion

A new Zn^{2+} fluorophore **10** (L^6) was synthesized that has advantages over the previously described Zn^{2+} probe **5** (L^5). The binding properties of **10** with Zn^{2+} were comparable to that for **5**, while Zn^{2+} sensitivity was improved considerably. We should note that the $\text{p}K_a$ value ($\text{p}K_a = \text{ca. } 10\text{--}11$) of 8-OH group of quinolinol moiety of **10** in the excited state is much higher than the corresponding $\text{p}K_a$ value in the ground state ($\text{p}K_a = 2.5$), which is much smaller than that of **9b** ($\text{p}K_a = 6.1$) having no cyclen unit, permitting a quantitative measurement of Zn^{2+} concentrations at neutral pH. A caged derivative of **12** (BS-caged- L^6) was also synthesized, and its uncaging properties were examined. The rapid uncaging of **12** by Zn^{2+} -dependent hydrolysis and Zn^{2+} -independent photolysis would be useful for Zn^{2+} sensing. Even more efficient hydrolytic uncaging may be possible by introducing additional electron-withdrawing groups on the quinoline ring.²⁴ In addition, the staining of HeLa cells containing **10** and **12** was successful. Attempts to sense Zn^{2+} in apoptotic cells are currently underway.

Acknowledgment. This work was supported by grants-in-aid from the Ministry of Education, Culture, Sports, Science and Technology (MEXT) of Japan (No. 18390009 and 19659026) and “Academic Frontier” project for private universities: matching fund subsidy from MEXT, 2009–2013. S.A. is grateful for grants from Mitsubishi Chemical Corporation Fund (Tokyo), the Terumo Life Pharmaceutical Research (Tokyo), the Novartis Foundation (Tokyo, Japan), the Naito Foundation (Tokyo), and the Tokuyama Science Foundation (Tokyo). M.K. is thankful for a grant-in-aid from MEXT of Japan (No. 20750081) and a Sasakawa Scientific Research Grant from the Japan Science Society.

Supporting Information Available: Figures S1–S9, tables, and CIFs for the X-ray crystal structure analysis of **10** ($\text{H}_2(\text{H}_{-1}\text{L}^6)$ (= HL^6)) and **11** ($\text{Zn}(\text{H}_{-1}\text{L}^6)$). This material is available free of charge via the Internet at <http://pubs.acs.org>.